RESIDUAL STRESS IN NB_3SN SUPERCONDUCTOR STRAND INTRODUCED BY STRUCTURE AND STOICHIOMETRIC DISTRIBUTION AFTER HEAT TREATMENT

Peng Jin[1], Lankai Li[2], Xide Li[3], Qiuliang Wang[4], Junsheng Cheng[5].

[1] Department of Engineering Mechanics, Tsinghua University, China, jp1527@126.com
[2] Institute of Electrical Engineering, Chinese Academy of Science, China, lkli@mail.iee.ac.cn
[3] Department of Engineering Mechanics, Tsinghua University, China, lixide@tsinghua.edu.cn
[4] Institute of Electrical Engineering, Chinese Academy of Science, China, qiuliang@mail.iee.ac.cn
[5] Institute of Electrical Engineering, Chinese Academy of Science, China, jscheng@mail.iee.ac.cn

Keywords: Superconductor strand, diffusion-induced stress, residual stress, Nb_3Sn

ABSTRACT

Nb_3Sn, a widely-adopted superconducting material, suffers from fragility and sensitivity to strain. An elongation of 0.7% may lead to the irreversible failure of Nb_3Sn strands. Therefore, the stress and strain analysis of superconductors has attracted much attention from researchers. Many studies have anticipated these drawbacks to be greatly influenced by thermal expansion mismatch between the Nb_3Sn superconducting phase and matrix. X-ray diffraction (XRD) stress analysis was executed on a heat treated bronze strand at room temperature and its average axial residual stress was measured to be −135.7 MPa with fluctuation of about 300 MPa. The considerable stress fluctuation phenomenon may originate from diffusion, which was supported by electron probe microanalysis (EPMA) results. This work highlights the importance of component distribution on the stress status of a superconducting strand, and can supplement the thermal mismatch model.

1 INTRODUCTION

Since discovered in 1911, superconductors experienced great development. New superconducting materials [1]–[7] continually produce new transition temperature records and better high-field performance, promoting the practical application of superconductors. Nevertheless, superconductivity is often modulated by strain or stress status. For example, an elongation of 0.7% may lead to the irreversible failure of Nb_3Sn strands [8], which are widely adopted in magnets for their high-field performance. Therefore, the stress analysis of superconductors has attracted much attention from researchers.

Research on stress analysis and superconductivity-strain relationship appears in large quantity, but the problem is still far from fully settled. Incorrect allowance may result in over prediction of cable performance [9]. Most study on SC strand emphasized the stress from thermal mismatch, especially during changes from room temperature [10, 11] or heat treatment temperature [11, 12] to working temperature. One of the commonly used assumptions is that stress will totally vanish at the reaction temperature and thermal mismatch will dominate the residual stress produced during the cooling process. It is very interesting that researchers adopting different plastic parameters and different models have obtained the same result that SC phases experience a 0.28% compression. Ahoranta et al. [13] considered more details about two- and three-dimensional geometries to develop various multiscale modeling skills, and discussed the heat treatment temperature at which the residual stress would vanish.

Recently, we conducted X-ray diffraction (XRD) stress analysis on a superconducting (SC) strand at room temperature. The average axial residual stress was −135.7 MPa with fluctuation of about 300 MPa. The XRD result did not seem to support the estimation of thermal mismatch, which predicted that the outer bronze shell should suffer a rather even and smooth tensile stress. Thus, there may be other

important factor affecting the stress in the strand besides the thermal mismatch. In fact, stoichiometric distribution may lead to such great fluctuation.

2 EXPERIMENTAL SETUP AND RESULTS

To measure the residual stress in an Nb_3Sn strand after heat treatment, XRD stress analysis (X-350A, Stress Technologies Co., Ltd, China.) was applied to a heat-treated bronze Nb3Sn strand (FSW-NSN-90, Furukawa Electric Co., Ltd., Japan) to test the normal stress along the axis of the strand. Electron probe X-ray microanalysis (JEOL JXA-8230, Japan) was also employed to inspect the local concentration of each component. The specimen was a single wire. The heat treatment schedule is: heat up by 1 K/h to 973 K, keep 973 K for 100 hours and then cool down to room temperature by 1 K/h.

2.1 XRD stress measurements

The specimen was fixed onto a two-dimensional translation stage which can move along both axial and transversal direction with a known distance between two tests. Axial translation of the stage controls the measuring position on the specimen and transversal translation helps ensure that the light spot lies exactly on the measuring position of the specimen. The specimen was slightly curved (deflection less than 1.0 mm, far smaller than the total axial length of 60.0 mm) because it was stored and transported as a coil. No efforts were made to straighten the strand, and the strand was handled carefully to ensure that no external loading or extra stress were introduced. Tested points were spaced along the axis at an interval of 10 mm. Each tested point was measured at least twice and the region around 30 mm was measured in detail.

The $\sin^2\psi$ analysis method was adopted in this work. The basic principle of this method is schematically illustrated in Fig. 1(a). When a specimen is loaded with tensile stress, it will elongate along the loading axis while shrinking perpendicularly to the loading direction because of Poisson's effect. The free surface of the specimen will undergo a two-dimensional stress status. If the specimen consists of small-enough grains, the interplanar distance of the lattice planes perpendicular to the external load will increase, while that of the lattice planes parallel to the external load (also parallel to surface of the specimen in this case) will decrease. Thus, measuring the diffraction angle from different incident angles will yield the stress in the strand. For a detailed derivation, please refer to Ref. [14]. Equation (1) gives the expression used to calculate the stress.

$$\sigma_x = -\left[E/\left(2(1+\nu)\right)\right]\cot\theta_0\left(\pi/180^\circ\right)\left(\partial 2\theta_{\phi=0^\circ}/\partial\sin^2\psi\right) \qquad (1)$$

where θ is the diffraction angle, ψ is the angle between the normal direction of the sample surface and the plane containing injection ray and reflection ray. The footnote ϕ denotes the angle between measurement direction and x axis. K is a constant determined by Young's modulus E, Poisson's ratio ν, original diffraction angle θ_0 (in degree) under experiment X-ray wave length and is usually available for common material in handbooks.

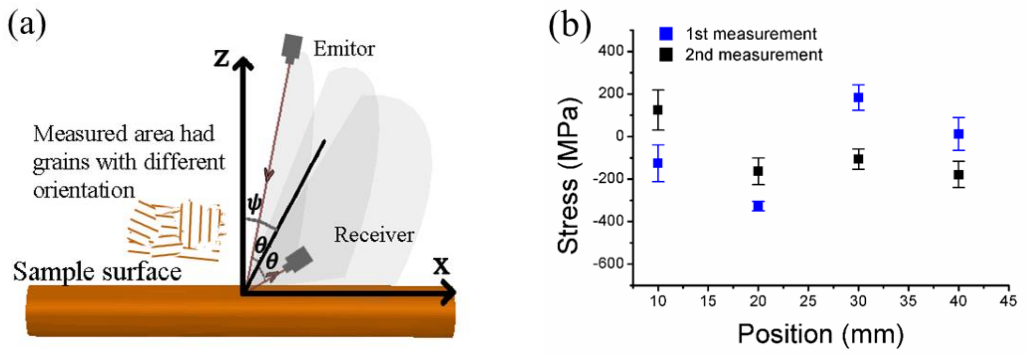

Figure 1: XRD stress measurements:
(a) Schematic of experimental setup, (b) axial stress measured by XRD.

This method adopts low-energy diffraction which is nondestructive, and relatively convenient. The stress value is calculated with a derivative, so knowing the standard peak position is not necessary. Uncertainty in the measurement is calculated from the deviation of the 2θ-$\sin^2\psi$ plot from a perfect line. The diffraction measurements were carried out at 0 °, 24.2 °, 35.3 °, and 45 °inclining angle. Because the signal obtained at each angle was weak, we employed a 2 ° waggling to improve the signal intensity. A Cr target was used. Bronze has a peak around 125.2 °with this target, and the corresponding stress constant is −444 MPa/°, adopted in this experiment. A spot size of 0.1 mm was selected, and the affected depth was 1 μm according to the manufacturer. The spot size is sufficiently small compared to the outer radius of the strand. In our tests the full width of half maximum (FWHM) usually lay between 1.1˚ to 2.1˚. Based on Scherrer's equation, the grain size ranges from 120 nm to 240 nm, comparatively small for this XRD test.

Fig. 1(a) shows the test principle and Fig 1(b) shows data with uncertainty within 80 MPa. The average of data listed in Fig 1(b) was −135.7 MPa along axis with a standard variation of 161 MPa. One fifth of the XRD results were well aligned, others were concave or zigzag-shaped on the other hand, XRD analysis of an unreacted strand of the same type revealed that the residual stress along the axis was 2 MPa±45 MPs, which is small compared with that of the heat-treated strand. To ensure the reliability of stress analysis using XRD technique, the comparing between theoretical analysis and experimental results only used the well-aligned 2θ-$\sin^2\psi$ plots to calculate stress in the following sections.

2.2 Local concentration from EPMA measurements

To observe the cross-section of the strand, we cut a piece of strand, embedded it in epoxy, and then polished it after XRD. The specimen was conductively coated with carbon. EPMA emits an ultra-thin electron beam that interacts with samples, causing them to emit X-rays at wavelengths characteristic to their component elements. EPMA can be applied to a point, a line, or an area, with precision from high to low. The precision of EPMA point analysis can be as high as 100 parts per million (ppm). Fig 2 shows the cross section of the tested specimen under optical microscope.

The use of EPMA has two main aspects of importance. First, material parameters are calculated or corrected with weighted averages. For bronze, Young's modulus and Poisson's ratio are calculated with empirical formulae [11]. For elastic parameters and thermal expansion coefficient, weighted averages are enough to describe the mechanical characteristics. Second, each component in the strand has a certain amount of impurities. The impurity elements will insert or embed themselves into the original lattice and distort it, resulting in strain as well as stress. So the stoichiometric distribution has a significant influence on the local stress status. This stress is described as diffusion induced stress in materials suffering from oxidation problems and lithium ion battery systems and has received much attention. The phenomenon widely exists in heterogeneous systems.

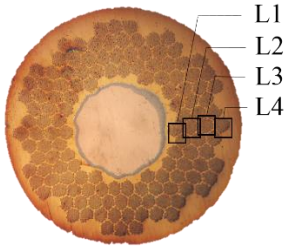

Figure 2: The cross section of the tested specimen under optical microscope.

Uneven composite concentration, which can be studied by electron probe microanalysis (EPMA), will also lead to diffusion stress [5]. EPMA results are shown in Table 1. We showed that each phase was actually a mixture of main components and others. For example, more than 3 at. % Ta existed in the Nb core, which may have had a positive role on reaction and grain size control. The superconducting phase had an atomic Nb-Sn ratio higher than 3:1, implying that some unreacted Nb may have been presented, while the bronze matrix contained remaining Sn. The Ta barrier separated the Nb and prevented it from reacting with Sn in the bronze matrix but was permeated by Cu. Taking the main

composition as the solvent and other elements as solutes, the concentration of the outer bronze shell had a standard deviation of 0.196%. The considerable stress fluctuation phenomenon may originate from diffusion, which was supported by electron probe microanalysis (EPMA) results.

	Nb (at. %)	Sn (at. %)	Ta (at. %)	Cu (at. %)
Bronze mantle	0.00	2.99	0.15	96.86
Matrix	0.59	1.82	0.20	97.39
Nb_3Sn phase	74.26	17.14	3.28	5.31
Unreacted Nb	91.48	0.95	3.55	3.97
Ta Barrier	0.91	0.00	92.74	6.33
Nb barrier	98.58	0.01	0.15	1.20
Copper core	0.00	0.02	0.15	99.78

Component in each area should sum up to be 100%. The possible error comes from incomplete possible element settings and facility errors.

Table 1: Typical EPMA results in each component.

3. THEORETICAL ANALYSIS

Thermal mismatch is well known to be an important factor in superconductor heat treatment processes, but only thermal mismatch alone cannot explain the stress fluctuation and concentration distribution may have the same importance.

From Table I, we can see that in Nb_3Sn phase and other material there exist a certain amount of impurities. The impurities may either replace atoms in original lattice or insert between lattice planes, or acting as inclusions, in either case resulting in volume mismatch and thus heterogeneity. Heterogeneity introduces residual stress in a structure, which is often ignored in general structural analysis. However, concentration gradient acts like a deformation mismatch. This is analogous to a well-constrained matrix containing inclusions of some size inserted randomly within the whole domain and thus leading to a certain amount of deformation, which will lead to a fluctuating stress field [15]. In axisymmetric systems, the stress-concentration relationship is

$$\sigma_D(r) = 2Er_c^{-2}\left(\int_0^{r_c} r'c(r')dr' - c(r)\right)\Big/\left(3(1-\upsilon)\right), \tag{9}$$

where $\sigma_D(r)$ is the axial stress as a function of position in the cross-section, $c(r)$ is local concentration in atom percentage, r_c is the radius of systems, E and ν are Young's modulus and Poisson's ratio, respectively.

For a more universal system, we altered (9) to

$$\sigma_D(\mathbf{p}) = (1/\Omega)\int_{A\in\Omega} c(\mathbf{p}')E(\mathbf{p}')/(3-3\upsilon(\mathbf{p}'))\,dA - c(\mathbf{p})E(\mathbf{p})/(3-3\upsilon(\mathbf{p})), \tag{10}$$

in which A is area and dA is infinitesimal area element at position $\mathbf{p}$, $c(\mathbf{p})$, $E(\mathbf{p})$, and $\nu(\mathbf{p})$ are all local material properties, and Ω represents the total cross-section. The estimated stresses in each component based on (10) often go up to several GPas, but will release during heat treatment, which will be discussed in the following section. However, heat treatment can not erase all the heterogeneity, and stress gradient in local area remains. When local concentration changes, stress should also follow (10) and change. The last column of Table 2 shows how much stress change is when local impurity volume percentage increase by 1%.

		Impurity volume (%)	Area weight (%)	Elastic modulus (GPa)	Poisson's ratio	Stress change (MPa)
L1	Nb	8.5%	1.8%	105.0	0.38	-530.3
	Nb_3Sn	29.1%	7.0%	126.1	0.32	-636.9
L2	Nb	12.3%	2.3%	105.0	0.38	-530.3

	Nb_3Sn	26.2%	10.8%	127.1	0.32	-641.8
L3	Nb	8.5%	2.2%	105.0	0.38	-530.3
	Nb_3Sn	19.8%	13.1%	129.0	0.32	-651.3
L4	Nb	9.5%	0.9%	105.0	0.38	-530.3
	Nb_3Sn	15.3%	10.0%	130.3	0.31	-658.1
Bronze matrix		3.7%	35.4%	128.2	0.34	-647.3
Nb barrier		1.4%	5.8%	105.0	0.38	-530.3
Ta barrier		7.2%	1.9%	180.0	0.34	-909.1
Copper core		0.2%	8.7%	128.1	0.34	-647.0

Table 2: stress change is when local impurity volume percentage increase by 1%

As mentioned above, EPMA shows that the concentration of the outer bronze shell had a standard deviation of 0.196%, from Table 2 we can predict the stress standard deviation due to concentration change is 126.9MPa.

4. DISCUSSIONS

From the results obtained above, we conclude that the stress field in an SC strand is affected not only thermal mismatch but also concentration distribution. Other possible factors include volume change mismatch and deformation history. Here we discuss some details of the experiments, and compare the influence from thermal mismatch with that of other mechanisms.

The influence of the original curvature of the sample was not salient. As mentioned, the deflection of the experimental sample is 1.0 mm over its total length of 60.0 mm, implying that its radius of curvature was 900 mm. Because the strand diameter was 0.80 mm, the residual strain introduced will be no more than 0.05%, negligible compared with that induced by stoichiometric factors.

Diffraction techniques were also adopted in previous studies, but as strain gauges rather than for typical stress analysis. X-rays ejected perpendicularly to the specimen axis can be used to directly obtain the lattice constants and compare them with standard values, which are often difficult to determine under different elemental compositions. In our analysis, we employed four diffraction measurements (two required at least) from different injection angles at each point. As a result, the stress measurement plots suffered from random disturbance less and could provide uncertainty information. However, large grains caused by the heat treatment can disturb the diffraction output.

XRD method is adopted in this paper to reveal the stress status, regardless of whether the measured area undergoes elastic or elasto-plastic deformation, although it is based on elastic theory. We take XRD as a convincible method because of two aspects. First, XRD stress analysis is feasible only where elasticity dominate. If the measured area exists high degree of plastic deformation, local lattice may change into disorder, XRD will not give out clear peak for calculation and we cannot analyze using this method. Second, plastic deformation and XRD test may happen at different scales. Plastic deformation is defined on macroscale, while XRD measures lattice spacing which has a smaller gauge length. Although from macroscale, one piece of area may deform plastically but some local tiny area within is still elastic, which will enable the XRD analysis. The local elastic zone should reach an equilibrium with surrounding plastic zones in stress. In this way, XRD reveals the real stress status.

Some XRD measurements and EPMA-based evaluations gave a stress value beyond the yielding stress, which may trigger additional confusion. Two possibilities can lead to this phenomenon: first, local stress status is hydrostatically dominant; second, when grain size is small enough, yielding stress can reach far beyond engineering yielding stress. In our experiments, local stress exceeding the yielding point is conceivable. The general yielding information is acquired through the engineering stress-strain relationship, which ignores necking and thus gives out a value smaller than reality. Since the measured grain size is 100 nm to 240 nm, the yielding strength can be as high as 400 MPa, according to Conrad**'s** work [16].High stress will persist until grains start sliding or rotating, leading to more a complicated stress status and a correspondingly complex XRD plot.

5 CONCLUSION

XRD and EPMA were used to study the residual stress in Nb_3Sn bronze strands experimentally. The XRD measurements showed that the mean axial residual stress in the sample was −135.7 MPa, with a fluctuation on the order of 300 MPa. EPMA revealed a concentration fluctuation along the samples surface. Taking diffusion into consideration explained the violent stress fluctuation, supported by the EPMA results. The results of FEM simulations considering the whole heat treatment process were consistent with the measured XRD average stress. This work highlights the importance of component distribution on the stress status of a superconducting strand, and can supplement the thermal mismatch model. It might be a new perspective to study stress and deformation of metal matrix composites by considering volume change and stoichiometric distribution.

ACKNOWLEDGEMENTS

This work was supported by the NSFC (Grant No. 11227202, 1147215, 51407176, 51477167), the National Basic Research Program of China (Grant Nos. 2013CB934203), and SRFDP (Grant No. 20130002110043).

REFERENCES

[1] W. A. Little, "Possibility of synthesizing an organic superconductor," *Physical Review*, vol. 134, 1964, p. A1416.
[2] D. Dijkkamp, T. Venkatesan, X. D. Wu, S. A. Shaheen, N. Jisrawi, Y. H. Min Lee, W. L. McLean, and M. Croft, "Preparation of Y−Ba-Cu oxide superconductor thin films using pulsed laser evaporation from high Tc bulk material," *Applied Physics Letters*, vol. 51, 1987, pp. 619-621.
[3] H. Maeda, Y. Tanaka, M. Fukutomi, and T. Asano, "A new high-Tc oxide superconductor without a rare earth element," *Japanese Journal of Applied Physics*, vol. 27, 1988, p. L209.
[4] S. Yamanaka, E. Enishi, H. Fukuoka, and M. Yasukawa, "High-pressure synthesis of a new silicon clathrate superconductor, Ba8Si46," *Inorganic chemistry*, vol. 39, 2000, pp. 56-58.
[5] V. Pantsyrny, A. Shikov and A. Vorobieva, "Nb_3Sn material development in Russia," *Cryogenics*, vol. 48, 2008, pp. 354-370.
[6] Y. Kamihara, T. Watanabe, M. Hirano, and H. Hosono, "Iron-Based Layered Superconductor La $[O_{1-x} F_x]$ FeAs (x= 0.05-0.12) with T c= 26 K," *Journal of the American Chemical Society*, vol. 130, 2008, pp. 3296-3297.
[7] Z. Du, D. Fang, Z. Wang, Y. Li, G. Du, H. Yang, X. Zhu, and H. Wen, "Anisotropic superconducting gap and elongated vortices with Caroli-De Gennes-Matricon states in the new superconductor $Ta_4Pd_3Te_{16}$," *Scientific reports*, vol. 5, 2015, 9408 EP-.
[8] R. Flükiger, D. Uglietti, C. Senatore, and F. Buta, "Microstructure, composition and critical current density of superconducting Nb_3Sn wires," *Cryogenics*, vol. 48, 2008, pp. 293-307.
[9] N. Mitchell, "Mechanical and magnetic load effects in Nb_3Sn cable-in-conduit conductors," *Cryogenics*, vol. 43, 2003, pp. 255-270.
[10] A. Nyilas, "Thermal contraction measurements of various materials using high resolution extensometers between 290 K and 7 K," in *ADVANCES IN CRYOGENIC ENGINEERING: Transactions of the International Cryogenic Materials Conference-ICMC*, 2004, pp. 151-158.
[11] N. Mitchell, "Finite element simulations of elasto-plastic processes in Nb_3Sn strands," *Cryogenics*, vol. 45, 2005, pp. 501-515.
[12] S. Murase and H. Okamoto, "FEM analysis of three directional strain states under applied tensile stress for various composite superconductors," *IEEE Trans. Appl. Supercond.*, vol. 14, 2004, pp. 1130-1133.
[13]M. Ahoranta, J. Lehtonen, T. Tarhasaari, and K. Weiss, "Modelling of local strain and stress relaxation in bronze processed Nb_3Sn wires," *Superconductor Science and Technology*, vol. 21, 2008, p. 025005.
[14] *ASM Handbook*, ASM International, Materials Park, OH, 1986, pp. 380-392.
[15] H. Haftbaradaran, J. Song, W. A. Curtin, and H. Gao, "Continuum and atomistic models of

strongly coupled diffusion, stress, and solute concentration," *Journal of Power Sources,* vol. 196, 2011, pp. 361-370.

[16] H. Conrad, "Grain size dependence of the plastic deformation kinetics in Cu," *Materials Science and Engineering: A,* vol. 341, 2003, pp. 216-228.